Electronic Supplementary Material (ESI) for Journal of Materials Chemistry A.

Supporting information for

Controllable Synthesis of 3D Binary Nickel-Cobalt Hydroxide/Graphene/Nickel Foam as Binder-free Electrode for High-performance Supercapacitors

Yang Bai, Weiqi Wang, Ranran Wang, Jing Sun*, and Lian Gao

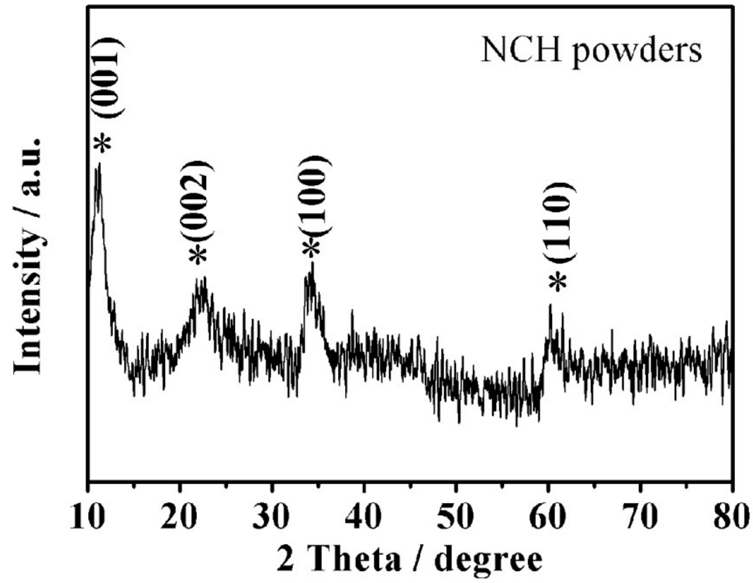

Fig. S1 XRD pattern of NCH powders scraped from NCH/G/NF electrodes.

Fig. S1 shows the XRD pattern of the NCH powders which were scraped from the NCH/G/NF electrodes. The pattern confirms the existence of Ni-Co binary hydroxides. It is well accepted that the $Ni(OH)_2$ has the similar structure and diffraction patterns with $Co(OH)_2$. Therefore, it is difficult to differentiate these two phases. The diffraction peaks of 11.3°, 22.6°, 34.5°, and 60.5° are corresponding to the (001), (002), (100), and (110) planes of $Ni(OH)_2$ and $Co(OH)_2$ phases, respectively. Similar results have been reported in previous literatures.[1-3]

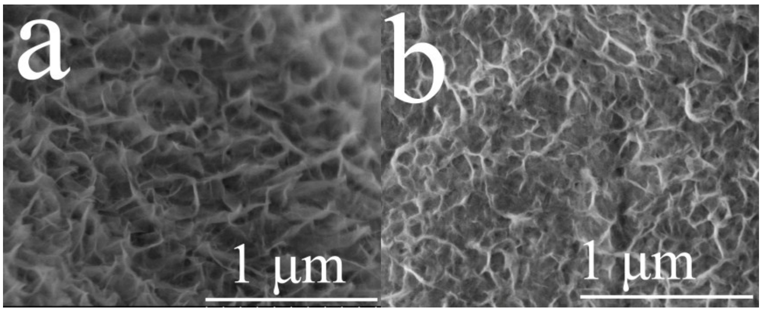

Fig. S2 The high magnification SEM images of NF (a) and NCH/NF (b)

Fig. S2 shows the SEM images of NF and NCH/NF with high magnification. Compared with NF, the size of NCH nanosheets is a little smaller than the nanosheets in the surface of NF. Meanwhile, the NCH composite displays the island structure, which is separated by some obvious boundaries.

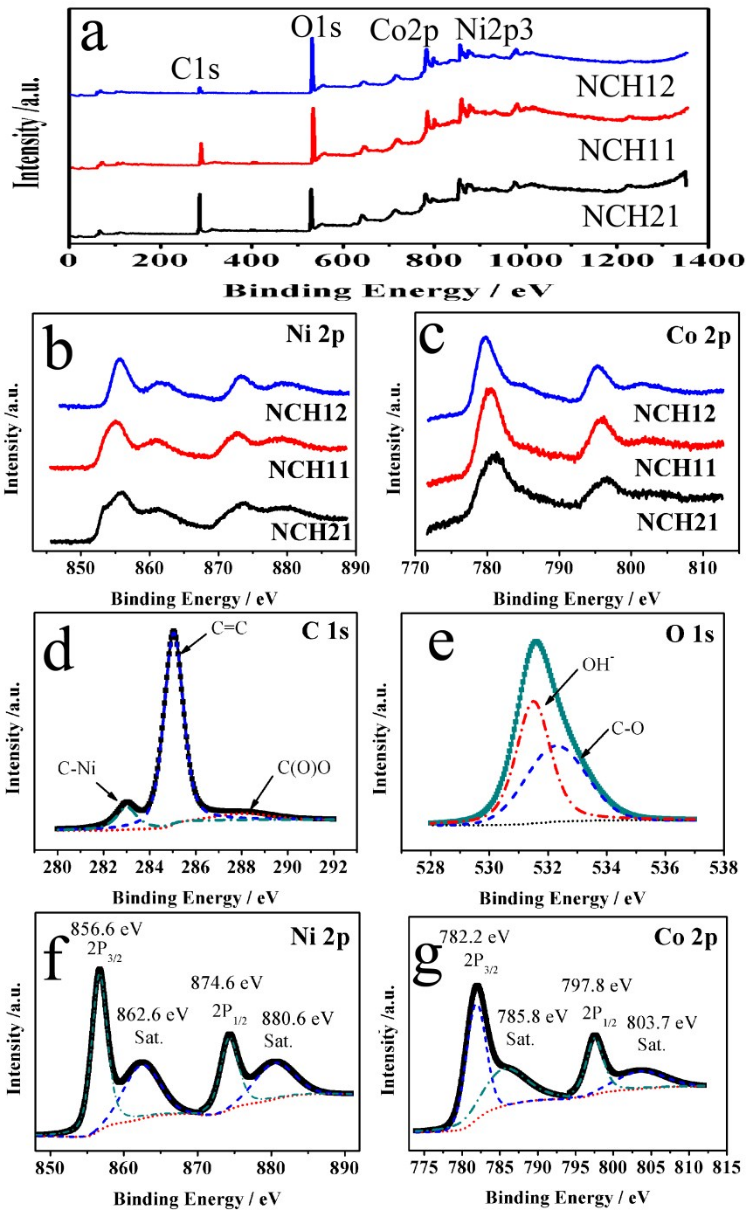

Fig. S3 XPS spectra of wide scan (a), Ni 2p (b) and Co 2p (c) for NCH/G/NF at different Ni/Co ratio and fitted XPS spectra of C 1s (d), O 1s (e), Ni 2p (f), and Co 2p (g) for NCH/G/NF electrode.

XPS was performed to illustrate the detailed information about elements and oxidation states of the as-prepared NCH/G/NF electrodes. The corresponding spectra are presented in Fig. S3. The bands observed in the wide scan spectra reveal the presence of C 1s, O 1s, Ni 2p and Co 2p in all the electrodes (Fig. S3a). As shown in Fig. S3b and c, the peaks of Ni 2p and Co 2p in all the three electrodes display a slight shift, which is caused by the difference of Ni/Co ratio. Fig. S3d exhibits the divided peaks of C 1s centered at 285.0 eV. The fitted peaks at 285.0 and 288.1 eV are attributed to the non-oxygenated ring C (C-C) and carboxylate carbon (C(O)O), respectively.[4, 5] The absorbance band intensities of the C(O)O is too much weaker than that of C-C, demonstrating the high quality of graphene. The peak at 283.1 eV is probably caused by the formation of C-Ni alloy during the CVD process. From Fig. S3e, it is observed that the broad peak of O 1s is centered at 532 eV, which is associated with bound hydroxide groups (OH^-) and confirms the formation of Ni-Co binary hydroxides.[6] The high resolution spectrum can be divided into two peaks at binding energies of 531.5 and 532.6 eV for OH^- and C-O.[7, 8] This result also supports the formation of NCH on the surface of graphene. As displayed in Fig. S3f, two spin-orbit doublets at 856.6 and 874.6 eV can be identified as Ni $2p_{1/2}$ and Ni $2p_{3/2}$ signals of Ni^{2+}, whereas the peaks (indicated as "Sat") are assigned to Ni^{3+}.[8, 9] Similar spin-orbit doublets and shakeup satellites peaks at 782.2, 797.8 and 785.8, 803.7 eV are characteristic of Co^{2+} and Co^{3+} (Fig. S3g).[10] The XPS shows the NCH is a composition of Ni^{2+}, Ni^{3+}, Co^{2+}, and Co^{3+}.

To further analyze the detailed microstructure of NCH/G/NF electrodes with different Ni/Co ratio, TEM images were taken (Fig. S4). It could be observed that all the NCH nanosheets display a transparent features and folding structures, illustrating that the nanosheets are ultrathin. The lateral size of these nanosheets is much larger than their thickness, leading to the curling and bending morphology. The dark strips are the wrinkles of the nanosheets. With the Ni/Co ratio increasing, the size of the nanosheets becomes larger and larger, which is associated with the results of the SEM. For further study, selected-area electron diffraction (SAED) was conducted to investigate the crystalline characteristics of NCH for different Ni/Co ratios (Fig. S4). All the samples show well-defined and sharply diffraction rings, meaning that the NCHs are polycrystalline. The characteristic crystal planes of NCHs can be indexed as the (110), (002), and (100) planes. With the Ni/Co ratio increasing, the (002) planes appears and becomes clear, demonstrating higher crystallinity of NCH12.

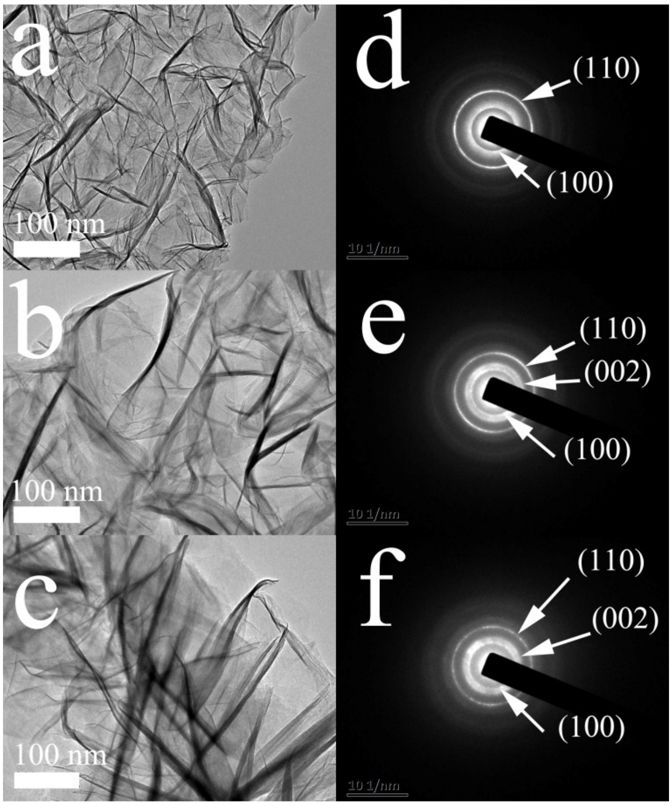

Fig. S4 TEM images of NCH/G/NF prepared in different Ni/Co ratio solutions, (a, d) NCH21/G/NF, (b, e) NCH11/G/NF and (c, f) NCH12/G/NF.

Table S1 Comparison of the maximum *Cs*, energy and average power densities based on active materials of some reported nickel-cobalt oxide (hydroxide)/nickel foam based pseudocapacitive materials and as-prepared electrode materials.

Electrodes	**Cs ($F\ g^{-1}$)**	**Capacitance retention**	**Rate capacity**	**Ref.**
CoO@NiHON/NF	798.3 (1.67 A g^{-1})	95% (2000 cycles)	88% 10 A g^{-1}	11
Co_3O_4-NiO/NF	853 (2 A g^{-1})	95.1 (6000 cycles)	88% 20 A g^{-1}	12
$NiCo_2O_4$ arrays/NF	891 (1 A g^{-1})	97.2% (8000 cycles)	70% 40 A g^{-1}	13
$NiCo_2O_4$ /NF	900 (2 mV s^{-1})	85% (1000 cycles)	52.2% 20 mV s^{-1}	14
Co-Ni oxide/NF	936 (5 mV s^{-1})	71.4% (10000 cycles)	60.4% 200 mV s^{-1}	15
$(Ni\text{-}Co)(OH)_2$ /$NiCo_2O_4$ /NF	1132 (2 mA cm^{-2})	90 % (2000 cycles)	61.8% 50 mA cm^{-2}	1
Ni-Co binary hydroxide/Graphene/NF	1410 (2 A g^{-1})	92.1 % (2500 cycles)	74.1% (20 A g^{-1})	This work
$Co_xNi_{1-x}(OH)_2$ /NF	1464.7 (1 A g^{-1})	86% (500 cycles)	73.7% 6 A g^{-1}	16
$NiCo_2O_4$@MnO_2/NF	1471 (2 mV s^{-1})	88% (1000 cycles)	50.1% 20 mV s^{-1}	14
Ni-Co LDHs/NF	1734 (6 A g^{-1})	86% (1000 cycles)	66.1% 30 A g^{-1}	17
$NiCo_2O_4$/NF	2000 (10 A g^{-1})	93.8% (10000 cycles)	53.4% 100 A g^{-1}	18
CoO-$NiCo_2O_4$/NF	2163 (1 A g^{-1})	75% (3000 cycles)	59.5% 20 A g^{-1}	19

Table S2 Comparison of the maximum *Cs*, energy and average power densities based on active materials of some reported nickel or cobalt oxide (hydroxide)/graphene based pseudocapacitive materials and as-prepared electrode materials.

Electrodes	**Cs (F g^{-1})**	**Capacitance retention**	**Rate capacity**	**Ref.**
NiO/Graphene sheets	400 (2 A g^{-1})	94% (2000 cycles)	81% 40 A g^{-1}	[20]
NiCoHCF/GO/Stainless steel	411 (0.2 A g^{-1})	83% (800 cycles)	44.3% 9 A g^{-1}	[21]
NiO/RGO	525 (0.2A g^{-1})	95.4% (1000 cycles)	65.1% 6 A g^{-1}	[22]
Graphene-$NiCo_2O_4$ composite	618 (5 mV s^{-1})	83.3% (10000 cycles)	53.5% 200 mV s^{-1}	[23]
$Co(OH)_2$/graphene/NF	694 (2 A g^{-1})	91.9% (3000 cycles)	72.9% 32 A g^{-1}	[3]
Sponge@rGO@$Co(OH)_2$	752 (5 mV s^{-1})	-	-	[24]
NiO/RGO	770 (2 mV s^{-1})	96% (1000 cycles)	46.2% 40 mV s^{-1}	[25]
Sponge@rGO@$Ni(OH)_2$	812 (5 mV s^{-1})	-	-	[24]
$NiCo_2O_4$/RGO composite	835 (1 A g-1)	86.5 % (4000 cycles)	71.8% 20 A g^{-1}	[26]
$NiCo_2O_4$–rGO	873 (0.5 A g^{-1})	89.3% (1500 cycles)	71.5% 20 A g^{-1}	[27]
$NiCo_2O_4$-RGO composite	882 (1 A g^{-1})	93.8% (3000 cycles)	69.1% 10 A g^{-1}	[28]
CoO-3D Graphene	980 (1 A g^{-1})	71.4% (7000 cycles)	61.2% 20 A g^{-1}	[29]
$NiCo_2O_4$–rGO	1222 (0.5 A g^{-1})	91.6% (3000 cycles)	77.7% 20 A g^{-1}	[30]
$Ni(OH)_2$/RGO	1335 (2.8 A g^{-1})	~110% (2000 cycles)	71.3% 45.7 A g^{-1}	[31]
Ni-Co binary hydroxide/Graphene/NF	1410 (2 A g-1)	92.1 % (2500 cycles)	74.1% 20 A g^{-1}	This work
Co_3O_4/Graphene/NF	1434 (1.5 A g^{-1})	94.1% (5000 cycles)	78.5% 7.5 A g^{-1}	[32]

References

1. X. Gong, J. P. Cheng, F. Liu, L. Zhang and X. Zhang, *Journal of Power Sources*, 2014, **267**, 610-616.
2. J. Yan, Z. J. Fan, W. Sun, G. Q. Ning, T. Wei, Q. Zhang, R. F. Zhang, L. J. Zhi and F. Wei, *Advanced Functional Materials*, 2012, **22**, 2632-2641.
3. C. Zhao, X. Wang, S. Wang, Y. Wang, Y. Zhao and W. Zheng, *International Journal of Hydrogen Energy*, 2012, **37**, 11846-11852.
4. H. Li, G. Zhu, Z.-H. Liu, Z. Yang and Z. Wang, *Carbon*, 2010, **48**, 4391-4396.
5. X.-L. Wu, L. Wang, C.-L. Chen, A.-W. Xu and X.-K. Wang, *Journal of Materials Chemistry*, 2011, **21**, 17353.
6. U. M. Patil, J. S. Sohn, S. B. Kulkarni, S. C. Lee, H. G. Park, K. V. Gurav, J. H. Kim and S. C. Jun, *ACS Applied Materials & Interfaces*, 2014, **6**, 2450-2458.
7. M. Zong, Y. Huang, Y. Zhao, X. Sun, C. Qu, D. Luo and J. Zheng, *RSC Advances*, 2013, **3**, 23638.
8. V. H. Nguyen and J.-J. Shim, *Journal of Power Sources*, 2015, **273**, 110-117.
9. J.-M. Song, J.-J. Ni, J. Zhang, D. Ling, H.-L. Niu, C.-J. Mao, S.-Y. Zhang and Y.-H. Shen, *Journal of Nanoparticle Research*, 2014, **16**.
10. H. Chen, L. Hu, M. Chen, Y. Yan and L. Wu, *Advanced Functional Materials*, 2014, **24**, 934-942.
11. C. Guan, J. Liu, C. Cheng, H. Li, X. Li, W. Zhou, H. Zhang and H. J. Fan, *Energy & Environmental Science*, 2011, **4**, 4496.
12. J. T. Xinhui Xia, Yongqi Zhang,Xiuli Wang,Changdong Gu,Xinbing Zhao,and Hongjin Fan, *ACS Nano*, 2012, **6**, 5531-5538.
13. X. Y. Liu, Y. Q. Zhang, X. H. Xia, S. J. Shi, Y. Lu, X. L. Wang, C. D. Gu and J. P. Tu, *Journal of Power Sources*, 2013, **239**, 157-163.
14. L. Yu, G. Zhang, C. Yuan and X. W. Lou, *Chemical communications*, 2013, **49**, 137-139.
15. H. W. Cho, J. H. Nam, J. H. Park, K. M. Kim and J. M. Ko, *Bulletin of the Korean Chemical Society*, 2012, **33**, 3993-3997.
16. X. Liu, J. Huang, X. Wei, C. Yuan, T. Liu, D. Cao, J. Yin and G. Wang, *Journal of Power Sources*, 2013, **240**, 338-343.
17. J. Pu, Y. Tong, S. Wang, E. Sheng and Z. Wang, *Journal of Power Sources*, 2014, **250**, 250-256.
18. Y. Chen, B. Qu, L. Hu, Z. Xu, Q. Li and T. Wang, *Nanoscale*, 2013, **5**, 9812-9820.
19. K. Jang, S. Yu, S.-H. Park, H.-S. Kim and H. Ahn, *Journal of Alloys and Compounds*, 2015, **618**, 227-232.
20. X. H. Xia, J. P. Tu, Y. J. Mai, R. Chen, X. L. Wang, C. D. Gu and X. B. Zhao, *Chem-Eur J*, 2011, **17**, 10898-10905.
21. S. Ghasemi, R. Ojani and S. Ausi, *International Journal of Hydrogen Energy*, 2014, **39**, 14918-14926.
22. B. Zhao, J. Song, P. Liu, W. Xu, T. Fang, Z. Jiao, H. Zhang and Y. Jiang, *Journal of Materials Chemistry*, 2011, **21**, 18792-18798.
23. H. Wang, C. M. B. Holt, Z. Li, X. Tan, B. S. Amirkhiz, Z. Xu, B. C. Olsen, T. Stephenson and D. Mitlin, *Nano Research*, 2012, **5**, 605-617.
24. D. P. Dubal, R. Holze and P. Gomez-Romero, *Scientific reports*, 2014, **4**, 7349.
25. X. Zhu, H. Dai, J. Hu, L. Ding and L. Jiang, *Journal of Power Sources*, 2012, **203**, 243-249.
26. W. HuanWen, H. ZhongAi, C. YanQin, C. YanLi, W. HongYing, Z. ZiYu and Y. YuYing, *Journal of Materials Chemistry*, 2011, **21**, 10504–10511.

27. X. Wang, C. Yan, A. Sumboja and P. S. Lee, *Journal of Nanoscience and Nanotechnology*, 2014, **14**, 7104-7110.
28. J. P. Wang, S. L. Wang, Z. C. Huang, Y. M. Yu and J. L. Liu, *Ceramics International*, 2014, **40**, 12751-12758.
29. Y. G. Zhu, Y. Wang, Y. M. Shi, Z. X. Huang, L. Fu and H. Y. Yang, *Advanced Energy Materials*, 2014, **4**, 1301788.
30. Y. C. Song, J. Wang, Z. S. Li, D. H. Guan, T. Mann, Q. Liu, M. L. Zhang and L. H. Liu, *Microporous And Mesoporous Materials*, 2012, **148**, 159-165.
31. H. L. Wang, H. S. Casalongue, Y. Y. Liang and H. J. Dai, *J Am Chem Soc*, 2010, **132**, 7472-7477.
32. V. Hoa Nguyen and J.-J. Shim, *Materials Letters*, 2015, **139**, 377-381.